Observation of Carrier-Density-Dependent Many-Body Effects in Graphene via Tunneling Spectroscopy

Victor W. Brar (韦小宝),[1,2] Sebastian Wickenburg (魏烈钢),[1] Melissa Panlasigui,[1] Cheol-Hwan Park,[1,2]
Tim O. Wehling,[3,4] Yuanbo Zhang (张远波),[1] Régis Decker,[1,2] Çağlar Girit,[1,2] Alexander V. Balatsky,[3] Steven G. Louie,[1,2]
Alex Zettl,[1,2] and Michael F. Crommie[1,2]

[1]*Department of Physics, University of California at Berkeley, Berkeley, California 94720, USA*
[2]*Materials Sciences Division, Lawrence Berkeley Laboratory, Berkeley, California 94720, USA*
[3]*Theoretical Division and Center for Integrated Nanotechnologies, Los Alamos National Laboratory,*
Los Alamos, New Mexico 87545, USA
[4]*1. Institut für Theoretische Physik, Universität Hamburg, D-20355 Hamburg, Germany*
(Received 4 November 2009; published 22 January 2010)

We find the scanning tunneling spectra of backgated graphene monolayers to be significantly altered by many-body excitations. Experimental features in the spectra arising from electron-plasmon interactions show carrier density dependence, distinguishing them from density-independent electron-phonon features. Using a straightforward model, we are able to calculate theoretical tunneling spectra that agree well with our data, providing insight into the effects of many-body interactions on the lifetime of graphene quasiparticles.

The electronic properties of graphene depend strongly on how its charge carriers interact with different many-body excitations, such as plasmons and phonons. Electron-hole (*e*-hole) generation, electron-plasmon (*e*-pl) interactions, and electron-phonon (*e*-ph) interactions play a strong role in both renormalizing graphene electronic structure and in creating new inelastic excitation tunneling channels [1–5]. Such effects have been examined previously using angle-resolved photoemission spectroscopy (ARPES) [1] and high-resolution electron energy loss spectroscopy [6] for graphene grown on SiC(0001) substrates. These measurements provide evidence that graphene exhibits band renormalization and anomalous lifetime effects related to *e*-pl and *e*-ph interactions, but they suffer from complications and alternate interpretations due to the complex and inhomogeneous SiC(0001) substrate [7,8]. In order to unravel the influence of many-body effects in graphene it is useful to explore graphene monolayers on alternate substrates, such as SiO_2, which interact differently and which can be electrically backgated [9] (thereby allowing graphene charge carrier density to be varied continuously). Scanning tunneling spectroscopy (STS) is a powerful technique for exploring many-body effects in such systems due to its subnanometer spatial resolution, its high energy resolution, its capability for measuring both filled and empty state features, and the ease with which it can be integrated with a tunable gate electrode [10–14].

Here we report STS measurements revealing the effects of many-body excitations on the electronic properties of backgated monolayer graphene flakes placed on a SiO_2 substrate. Plasmon and phonon effects are both clearly observed and resolved through the use of gate-tunable changes in graphene charge carrier density n. Two distinct classes of spectroscopic features are observed as n is varied

through application of a backgate voltage V_g. The first type of feature shifts in energy with varying gate voltage, while the second is gate-independent. *Ab initio* calculations indicate that the first type of feature is due to many-body renormalization of the quasiparticle self-energy, while the second type is caused by inelastic tunneling via phonons. Comparison between theory and experiment allows us to directly resolve the influence of plasmon and phonon excitations on quasiparticle lifetimes in graphene.

Our measurements were performed in an Omicron LT-STM operating at 4.2 K and using electrochemically etched W and PtIr tips. Graphene samples were exfoliated on a 285 nm thick SiO_2 layer atop a heavily doped Si crystal which was used as a backgate [9]. In order to avoid spurious tip contamination, the tips of the scanning tunneling microscope (STM) were calibrated spectroscopically against the Shockley surface state on either a Cu(111) or Au(111) surface both before and after graphene measurement [7] (reported spectra were reproduced with numerous samples and tips prepared this way). dI/dV signals were measured under open feedback conditions by lock-in detection of the ac tunneling current modulated by a 300–400 Hz, 10–15 mV (rms) signal added to the tunneling bias (the bias voltage V_b here is defined as the sample potential referenced to the tip). d^2I/dV^2 measurements were made simultaneously by lock-in detection of the second harmonic of the ac tunneling current.

Figure 1(a) shows a typical dI/dV curve obtained with a backgate voltage of $V_g = +20$ V (the electron-doped regime). In order to better resolve the many-body features in this spectra the second derivative of the tunnel current, d^2I/dV^2, is also displayed. This shows a number of dips in the filled states ($V_b < 0$) and peaks in the empty states ($V_b > 0$). The dependence of these features on V_g (i.e., on
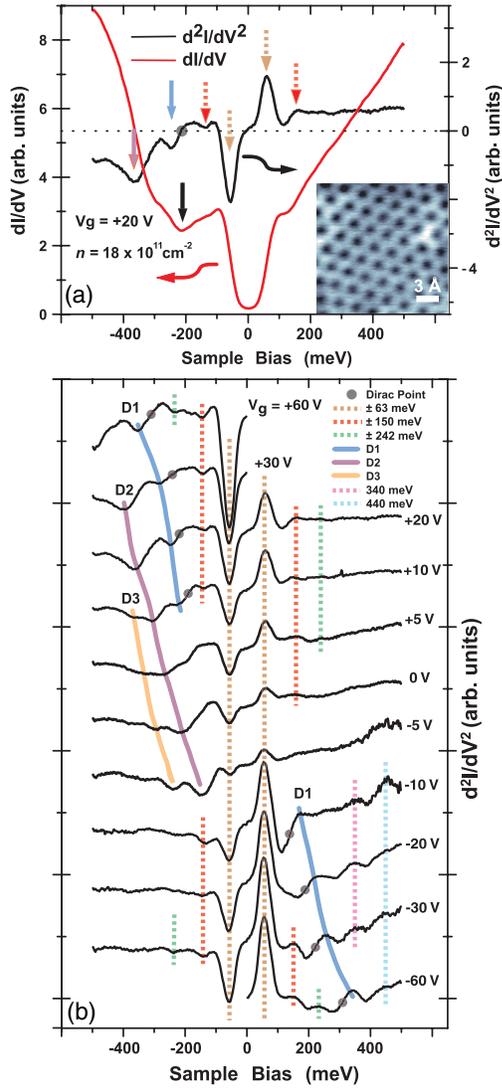
FIG. 1 (color). (a) dI/dV and d^2I/dV^2 spectra of graphene monolayer on SiO$_2$ with $V_g = +20$ V (junction parameters: 0.5 V, 0.12 nA, $T = 4.2$ K). Black arrow indicates minimum in dI/dV due to Dirac point (corresponding point in d^2I/dV^2 is shown with gray dot). Inset: STM topograph showing typical graphene surface quality for this study. (b) d^2I/dV^2 measurements taken at same point on the graphene surface for different gate voltages (V_g) (junction parameters: ±0.5 V, 0.12 nA, 4.2 K). Non-carrier-density-dependent features are tracked with dashed colored lines. Carrier-density-dependent features are labeled D1, D2, and D3, and are tracked with solid colored lines.

charge carrier density n) can be seen in Fig. 1(b). Two distinct types of behavior are seen: one class of features (tracked with solid colored lines) shift in energy with varying V_g while the other (tracked with dashed colored lines) does not.

Features in d^2I/dV^2 associated with many-body interactions have been previously observed in STS spectra on different surfaces [10–13,15], but this is the first time that such STS features have been observed as a function of

surface charge carrier density. Here we explain the cause of these features in graphene, including why some features show n dependence and some do not.

We first discuss the gate-independent features, which we attribute to phonon-mediated inelastic tunneling. A sign of inelastic tunneling is the presence of antisymmetric peaks in d^2I/dV^2 on opposite sides of the Fermi energy [14]. Such features can be seen in Fig. 1(b) at ±63, ±150, and ±242 mV. The 63 mV feature, described in previous work [16], arises from phonon-mediated inelastic tunneling via a K-point phonon. The large inelastic signal from this process mimics the appearance of a 126 meV gap at the Fermi level, consistent with previous analysis [17]. The new 150 mV feature observed here correlates well in energy with another K-point graphene phonon [18], and so we hypothesize that this feature is similarly due to inelastic tunneling.

In order to test this hypothesis we performed a frozen phonon calculation within the framework of density functional theory [17] to determine if the 150 meV K-point graphene phonon could be the cause of this increase in tunnel current. We find that this is, indeed, the case via mixing of the π bands at the K point with π and nearly free electron bands at the Γ point. Our results show that for a STM tip ~4 Å above a graphene sheet the inelastic conductance change due to the 150 meV phonon should have a magnitude equivalent to 7% of the inelastic tunneling signal due to the 63 meV phonon. This is consistent with the relative amplitudes of the two features shown in Fig. 1, thus providing support for an inelastic phonon-based origin of the 150 meV feature. Such an explanation, however, does not easily apply to the 242 meV feature, which has an energy 40 meV higher than the most energetic phonon found in graphene. One possible explanation for this feature is that it arises from multiphonon processes. It is interesting to compare the spectroscopic features seen here with spectroscopic features seen previously for the surface of bulk graphite. The low-energy feature seen here at 63 meV is similar to features seen in graphite [13,15,19], but features with a higher energy magnitude do not compare well.

We now discuss the gate-dependent spectral features [labeled in Fig. 1(b) as D1, D2, and D3]. Although it is tempting to attribute these to plasmon-assisted inelastic tunneling (since the plasmon energy is dependent on carrier density), this explanation is inconsistent with the fact that they appear only on one side of the Fermi energy for a particular doping. An alternative explanation is that these features arise due to e-pl and e-ph renormalization of the quasiparticle self-energy. Such an explanation would be consistent with recent ARPES experiments [1] and theoretical predictions [2,3,5]. To test this idea, we calculated how plasmon and phonon-induced scattering processes influence STM dI/dV spectra, and we compared the results to our experimental data. To do this we used (and expanded upon) a model previously applied to interpret STS spectra of metallic surface states [10,12].

This model relates the elastic (i.e., renormalized) component of the STM tunneling conductance to the imaginary part of the quasiparticle self-energy [$\text{Im}\Sigma(\varepsilon)$] [10,12]:

$$\frac{dI}{dV}_{\text{elastic}}(V) = \frac{C}{\pi} \int \frac{\text{Im}\Sigma(|\mathbf{k}| = \varepsilon/\hbar v_f, \varepsilon) \times \text{DOS}(\varepsilon) d\varepsilon}{(eV - \varepsilon)^2 + \text{Im}\Sigma(|\mathbf{k}| = \varepsilon/\hbar v_f, \varepsilon)^2}.$$

(1)

Here ε is the graphene quasiparticle energy and $\text{DOS}(\varepsilon)$ is the bare graphene density of states, given by $8\pi\varepsilon/\hbar v_f$ (v_f is the Fermi velocity in graphene). C is the bare tunneling matrix element (which includes tip geometry). We assume in the above expression that the spectral density for electronic quasiparticles in graphene, $A(\mathbf{k}, \varepsilon)$, can be approximated by a Lorentzian centered at $\varepsilon = \hbar v_f |\mathbf{k}|$ with a width (FWHM) given by $2\,\text{Im}\Sigma(|\mathbf{k}| = \varepsilon/\hbar v_f, \varepsilon)$, and that there is negligible energy dependence in C for the energy range considered. In order to obtain the interacting quasiparticle self-energy, we performed an *ab initio* on shell calculation for graphene within a *GW* approximation similar to that in Ref. [3]. Here we model a suspended graphene sheet with appropriate doping and calculate $\text{Im}\Sigma(|\mathbf{k}| = \varepsilon/\hbar v_f, \varepsilon) \equiv \text{Im}\Sigma(\varepsilon)$ along the K-Γ direction in reciprocal space (our results are not significantly altered if we use an average of quasiparticle self-energies along the K-Γ, K-M, and K-K directions in reciprocal space). The inset of Fig. 2 shows the resulting theoretical $\text{Im}\Sigma(\varepsilon)$ with separate contributions from *e-e* interactions (*e*-hole excitations and plasmons) and *e-ph* interactions. The green line in Fig. 2(a) shows the expected dI/dV signal of an electron-doped graphene sample when no many-body interactions are considered. dI/dV is then simply proportional to the bare (noninteracting) local density of states (LDOS) of graphene, and has a "V" structure that goes to zero at the Dirac point energy (E_D). The blue line in Fig. 2(a) shows the theoretical elastic (i.e., renormalized) component of dI/dV when interactions are included through our calculated $\text{Im}\Sigma(\varepsilon)$ in Eq. (1). The interacting dI/dV differs from the noninteracting case in two important ways: (1) the dI/dV signal becomes finite at the Dirac point energy and (2) kinks appear in the dI/dV signal that are absent in the bare LDOS for graphene.

In order to directly compare the theoretical dI/dV to our experimental results, we must also include inelastic tunneling channels. The effect of inelastic tunneling processes on the tunneling signal is to increase tunnel conductance as follows [20]:

$$\Delta\frac{dI}{dV}_{\text{inelastic}}(V) = \sum_i \frac{\lambda_i}{\sigma_i \sqrt{2\pi}} \left| \int_0^{eV} \frac{dI}{dV}_{\text{elastic}}(eV - \varepsilon) \right.$$
$$\left. \times\, e^{-(|\varepsilon| - \hbar\omega_i)^2/2\sigma_i^2} d\varepsilon \right|.$$

(2)

Here $\hbar\omega_i$ is the energy of the ith inelastic excitation, σ_i is the energy width of this inelastic feature, and λ_i is the electronic coupling constant to the ith excitation. The net result of inelastic tunneling processes is to add satellites of
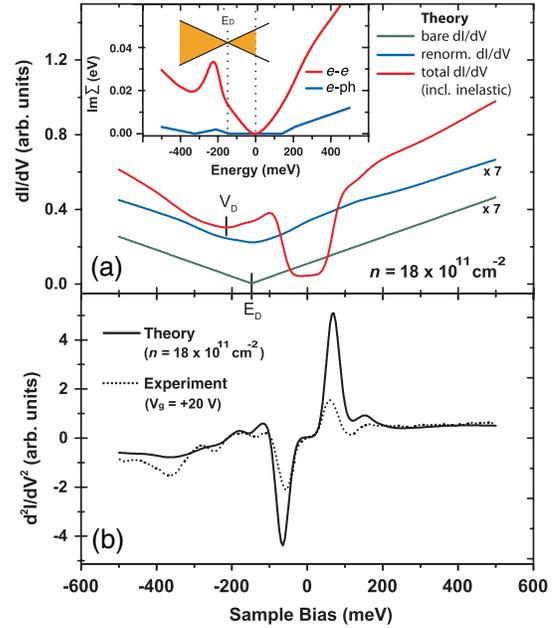

FIG. 2 (color).   (a) Green line shows theoretical elastic tunneling conductance (dI/dV) of graphene with no many-body interactions present. Blue line shows theoretical elastic component of dI/dV for graphene including many-body interactions. Red line shows total theoretical dI/dV for graphene including both elastic and inelastic tunneling processes. The blue curve and the green curve have been multiplied by a factor of 7 for easier viewing; all three curves share a common origin. Inset: Calculated $\text{Im}\Sigma(\varepsilon)$ for graphene quasiparticles along the Γ-K direction due to *e-e* (red line) and *e-ph* (blue line) interactions. (b) Solid line shows normalized theoretical d^2I/dV^2 for graphene including both elastic and inelastic processes as in (a). Dotted line shows experimental d^2I/dV^2 measurement of graphene with $V_g = +20$ V (corresponding to $n = 18 \times 10^{11}$ cm^{-2} used in the theoretical calculation).

the elastic signal at voltages $\pm\frac{\hbar\omega_i}{e}$ with respect to E_F [20]. The total dI/dV [shown in red in Fig. 2(a)] is simply the sum of the elastic and inelastic components. $\lambda_{63\,\text{meV}}$ was determined experimentally in previous work to be ~ 10 [16], while the ratio $\lambda_{63\,\text{meV}}/\lambda_{150\,\text{meV}}$ is found theoretically in this work to be ~ 15. σ_i is experimentally determined to be 17 meV for both phonons. Our final theoretical total dI/dV and d^2I/dV^2 curves are shown in Figs. 2(a) and 2(b), respectively. For comparison to experiment we have also plotted an experimental d^2I/dV^2 curve with appropriate graphene charge carrier density in Fig. 2(b). The main features seen in the experimental d^2I/dV^2 curve are reproduced in the theoretical curve, although there is some discrepancy in the relative feature magnitudes.

We have compared our experimentally observed d^2I/dV^2 spectra with calculations for many different doping conditions (Fig. 3). In each case $\text{Im}\Sigma(\varepsilon)$ was calculated as before, and Eqs. (1) and (2) were used to ascertain the resulting d^2I/dV^2 curve. The results of these calculations are shown in Fig. 3(b) alongside experimental curves
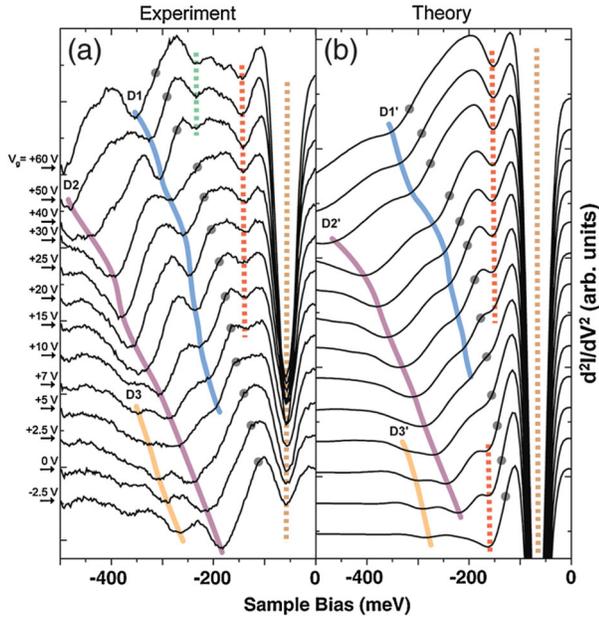
FIG. 3 (color). Comparison between (a) experimental and (b) theoretical d^2I/dV^2 versus sample bias in the filled states of graphene for different gate voltages (V_g) and corresponding electron densities (experimental junction parameters: -0.5 V, 0.12 nA, 4.2 K). Dispersive features D1' and D2' in (b) are known to arise from electron-plasmon interactions, while dispersive feature D3' is known to arise from electron-phonon interactions (dispersive features are tracked with solid colored lines as a guide to the eye). Nondispersive features in (b) (tracked with dashed colored lines as a guide to the eye) are known to arise from phonon-mediated inelastic tunneling channels. Solid gray dots mark the position of the Dirac point (V_D) for different gate voltages [Fig. 3(a)] and corresponding electron densities [Fig. 3(b)].

[Fig. 3(a)] for corresponding backgate voltages. Strong qualitative agreement can be seen in the gate dependence of the experimental and theoretical d^2I/dV^2 spectral features.

Armed with the insights gained through our theoretical modeling, we can now begin to understand the origins of the specific experimental dispersive features displayed in Figs. 1(b) and 3(a). Features D1 and D2 both originate from the anomalous peak in the self-energy of the graphene quasiparticles seen just below E_D in Fig. 2(a) inset (red curve). This peak in $\mathrm{Im}\Sigma(\varepsilon)$ arises due to plasmons in graphene that strongly scatter holes from below the Dirac point to the upper bands, thus drastically reducing the hole lifetime [1–3,5]. Feature D3 arises from a minimum in the phonon contribution to the self-energy [Fig. 2(a) inset, blue curve] in which $\mathrm{Im}\Sigma(\varepsilon)$ goes to zero at about 180 meV below the Dirac point. Although phonon-related, feature D3 disperses with carrier density because it correlates with the rate that quasiparticles are scattered by phonons to states near the density-dependent Dirac point energy [3].

While the majority of spectral features observed in our data are accounted for within this framework, there are still

some mysteries. First, the features observed in our experimental d^2I/dV^2 curves in Fig. 3(a) tend to be sharper than the theoretically predicted features in Fig. 3(b). This can be partially explained if graphene quasiparticles have a longer overall lifetime than calculated in our model. This might arise from structure in the spectral function, $A(\mathbf{k}, \varepsilon)$, not accounted for in our Lorentzian approximation [5]. Second, there are some carrier-density-independent features that do not correlate with known phonon energies. These include the previously mentioned nondispersive feature at ± 242 meV. Perhaps more difficult to explain are the two nondispersive modes seen at 340 and 440 meV only in the empty states for hole-doped samples. These features do not have antisymmetric counterparts about E_F and do not obviously correspond to important graphene excitations. The origin of these features is unclear at this time.

In conclusion, we have observed a number of reproducible many-body features in the d^2I/dV^2 tunneling spectra of graphene. By measuring the carrier-density-dependent properties of these features and applying a straightforward theoretical model we are able to distinguish plasmon-related features from phonon-related features, as well as inelastic effects from anomalous lifetime effects.

[1] A. Bostwick *et al.*, Nature Phys. **3**, 36 (2007).
[2] E. H. Hwang and S. Das Sarma, Phys. Rev. B **77**, 081412 (2008).
[3] C.-H. Park *et al.*, Phys. Rev. Lett. **102**, 076803 (2009).
[4] C.-H. Park *et al.*, Nano Lett. **9**, 4234 (2009).
[5] M. Polini *et al.*, Phys. Rev. B **77**, 081411 (2008).
[6] Y. Liu *et al.*, Phys. Rev. B **78**, 201403 (2008).
[7] V. W. Brar *et al.*, Appl. Phys. Lett. **91**, 122102 (2007).
[8] S. Y. Zhou *et al.*, Nature Mater. **6**, 770 (2007).
[9] K. S. Novoselov *et al.*, Science **306**, 666 (2004).
[10] A. Bauer *et al.*, Phys. Rev. B **65**, 075421 (2002).
[11] J. Kliewer *et al.*, Science **288**, 1399 (2000).
[12] J. Li *et al.*, Phys. Rev. Lett. **81**, 4464 (1998).
[13] D. P. E. Smith, G. Binnig, and C. F. Quate, Appl. Phys. Lett. **49**, 1641 (1986).
[14] B. C. Stipe, M. A. Rezaei, and W. Ho, Science **280**, 1732 (1998).
[15] L. Vitali *et al.*, Phys. Rev. B **69**, 121414 (2004).
[16] Y. Zhang *et al.*, Nature Phys. **4**, 627 (2008).
[17] T. O. Wehling *et al.*, Phys. Rev. Lett. **101**, 216803 (2008).
[18] M. Mohr *et al.*, Phys. Rev. B **76**, 035439 (2007).
[19] N. Agraït, J. G. Rodrigo, and S. Vieira, Ultramicroscopy **42–44**, 177 (1992).
[20] J. Lambe and R. C. Jaklevic, Phys. Rev. **165**, 821 (1968).